EFFECTS OF MSLA PRINTING PARAMETERS ON THE MECHANICAL AND ACOUSTIC PROPERTIES OF 3D-PRINTED RESIN FOR ULTRASONIC WEDGES

M.N.F. Saniman[1*], S.A. Zulkifli[1], M.R. Rahim[1], A. Zhahir[2], A. Ibrahim[3] and M.H. Muhammad Sidik[4]

[1]Mechanical Engineering Section, Malaysia France Institute, Universiti Kuala Lumpur, Section 14, 43650, Bandar Baru Bangi, Selangor, Malaysia.

[2]Department of Aerospace Engineering, Faculty of Engineering, Universiti Putra Malaysia, 43400 UPM Serdang, Selangor, Malaysia.

[3]Faculty of Mechanical Technology and Engineering, Universiti Teknikal Malaysia Melaka, Hang Tuah Jaya, 76100 Durian Tunggal, Melaka, Malaysia.

[4]Faculty of Mechanical and Automotive Engineering Technology, Universiti Malaysia Pahang Al-Sultan Abdullah, 26600 Pekan, Pahang, Malaysia.

*Corresponding Author's Email: mnfarhan@unikl.edu.my

Article History: Received 18 January 2026; Revised 27 June 2026; Accepted 12 July 2026

ABSTRACT: Additive manufacturing offers new opportunities to fabricate customized ultrasonic wedges for Non-Destructive Testing (NDT). However, the relationship between Stereolithography (SLA) printing parameters and the resulting mechanical and acoustic performance of printed wedges remains insufficiently understood. In this study, the effects of Layer Height (LH), Exposure Time (ET), and Light-off Delay (LD) on the mechanical and ultrasonic properties of SLA-printed polymer specimens were investigated using Response Surface Methodology (RSM) with a Central Composite Design (CCD). The compressive strength of the printed specimens ranged from 22 MPa to 79 MPa, indicating a strong dependence on the printing parameters. Ultrasonic attenuation ranged from 0.04 dB/mm to 0.17 dB/mm and generally increased with mechanical strength, suggesting a trade-off between mechanical integrity and acoustic transmission. A scatter-based mechanical–acoustic analysis further revealed that parameter conditions that produce higher compressive strength tend to result in slightly higher ultrasonic attenuation, due to increased polymer cross-link density and internal scattering mechanisms. The ultrasonic wave velocity exhibited a relatively small variation across the investigated parameter space, ranging from approximately 1970 m/s to 2150 m/s (≈ ±4% variation). A stepwise regression model based on LH and LD was developed to estimate ultrasonic velocity, which may serve as an initial estimator for wedge calibration prior to final experimental adjustment. Overall, the results demonstrate that SLA printing parameters can be optimized primarily based on mechanical–acoustic performance, while ultrasonic velocity remains relatively stable and can be calibrated within a narrow range. These findings provide practical guidance for the design and fabrication of SLA-printed ultrasonic wedges for NDT applications.

KEYWORDS: *Stereolithography (SLA); Ultrasonic Testing (UT); Response Surface Methodology (RSM); Ultrasonic Attenuation; Ultrasonic Velocity*

1.0 INTRODUCTION

Ultrasonic Testing (UT) has long been relied upon for structural integrity assessment in safety-critical industries. As Additive Manufacturing (AM) becomes increasingly embedded in engineering practice, ultrasonic techniques have also begun to play a greater role in evaluating printed components [1]. Unlike conventionally processed materials, additively manufactured parts often contain microstructural irregularities, layer interfaces, and directional features that can influence wave propagation. Consequently, ultrasonic velocity, attenuation, and scattering characteristics have become valuable indicators of internal consistency and structural reliability in printed materials [2]–[5].

Notably, in practical ultrasonic inspection systems, the wedge is not merely an accessory component. It governs the beam entry angle, stabilizes the coupling, and controls the initial energy transmission path into the test specimen. Conventional wedges are typically machined from acrylic or engineering polymers. Although machining offers dimensional precision, it also restricts geometric freedom and slows down customization. With the rapid advancement of AM, particularly polymer-based technologies, it is now technically feasible to fabricate wedges directly through 3D printing. Early studies demonstrated that polymer-based printed wedges can support ultrasonic wave propagation under controlled configurations [6]. However, much of this work has focused on thermoplastics produced via filament extrusion, while high-resolution photopolymer systems remain less explored in this context.

Moreover, vat photopolymerization technologies, including Stereolithography (SLA), Digital Light Processing (DLP), and Masked Stereolithography (MSLA), provide finer surface finishes and higher dimensional resolution than extrusion-based methods [7, 8]. The process relies on spatially controlled light exposure to initiate polymer cross-linking, and subtle variations in Exposure Time (ET), layer thickness, and curing conditions can significantly alter final mechanical properties [9, 10]. Numerous investigations have confirmed that build orientation, interlayer bonding, and post-curing protocols influence tensile, compressive, and flexural responses of printed photopolymer components [11]–[15]. In many cases, anisotropic behavior was observed, arising from layer-wise fabrication and incomplete polymer network development [16, 17].

Post-curing, in particular, has been indicated to modify stiffness, hardness, and brittleness through additional cross-link formation [11, 18, 19]. Studies examining solvent treatment and ultra-violet (UV) exposure duration have reported measurable differences in tribological performance and dimensional stability [20, 21]. On the other hand, calibration strategies aimed at compensating light-intensity non-uniformity and exposure variability have significantly reduced dimensional errors in MSLA systems [22, 23]. These findings collectively suggest that mechanical reliability in vat photopolymerization is strongly dependent on process control rather than material formulation alone.

Parallel to mechanical optimization research, a growing body of work has investigated the acoustic behavior of 3D printed polymers. Experimental measurements of phase velocity and frequency-dependent attenuation reveal that photopolymer materials exhibit measurable dispersion and energy loss characteristics in the megahertz range [4, 24]. Other than that, ultrasound-based characterization of viscoelastic properties further demonstrates that both longitudinal and transverse wave responses are sensitive to subtle differences in curing conditions and material formulation [25]. More recent studies have emphasized acoustic anisotropy in additively manufactured components, revealing that directional elastic variations can influence

echo amplitude and inspection reliability [5]. Additionally, in-situ ultrasonic monitoring approaches have highlighted the direct coupling between curing evolution and acoustic response during vat photopolymerization [26, 27].
Nevertheless, despite these advances, two research streams have largely evolved in isolation. Mechanical studies typically optimize strength or dimensional accuracy without assessing acoustic transmission performance [12, 13, 16, 22, 28]. Conversely, ultrasonic investigations frequently characterize wave propagation without linking results to specific MSLA parameter regimes [24–26, 29]. For ultrasonic wedge applications, this separation becomes problematic. A wedge must withstand probe pressure and operational loading and transmit ultrasonic energy consistently and predictably. Note that mechanical adequacy alone does not guarantee acoustic suitability.

Furthermore, the broader expansion of functional and smart photopolymer systems further underscores the need for integrated evaluation frameworks [30]. AM has already demonstrated its ability to tailor mechanical response through architectural design and material engineering [31, 32]. However, the translation of these capabilities into ultrasonic tooling applications has not been systematically examined. In particular, the combined influence of layer thickness, ET, and post-curing conditions on both compressive strength and ultrasonic transmission within wedge geometries remains insufficiently documented.

Therefore, this study explores the feasibility of using MSLA-fabricated resin wedges for UT applications. By experimentally evaluating compressive mechanical performance alongside longitudinal ultrasonic transmission characteristics, the work establishes a direct link between process parameters and functional acoustic behavior. The objectives of this study are to investigate the effects of Layer Height (LH), Exposure Time (ET), and Light-off Delay (LD) on compressive strength, ultrasonic wave velocity, and attenuation, and to examine the relationship between mechanical and acoustic performance. These objectives aim to demonstrate printability while defining performance boundaries that determine the suitability of 3D-printed resin wedges for Non-Destructive Testing (NDT) applications.

2.0 METHODOLOGY

2.1 Experimental Design and Statistical Framework

A Response Surface Methodology (RSM) based on a face-centered Central Composite Design (CCD) was employed to evaluate the influence of MSLA processing parameters on the mechanical and acoustic performance of printed ABS photopolymer specimens. Specifically, three independent variables with three levels were investigated: Layer Height (LH), Exposure Time (ET), and Light-off Delay (LD), as given in Table 1. These parameters directly control layer formation, curing progression, and interlayer stabilization during photopolymerization.

Table 1: MSLA printing parameter levels

Parameter	Symbol	Coded Value		
		Low (−1)	Center (0)	High (+1)
Layer height (mm)	LH	0.01	0.105	0.2
Exposure time (s)	ET	0.001	0.0505	0.1
Light-off delay (s)	LD	0	0.025	0.05

For a three-factor face-centered CCD, the experimental design consisted of eight factorial points, six axial points, and six replicated center points, yielding a total of 20 distinct parameter combinations, as presented in Table 2. The inclusion of replicated center points enabled estimation of pure experimental error and provided a basis for evaluating lack of fit in the regression model.

In RSM, a second-order polynomial regression model was used for each response variable. Statistical analysis was conducted using Minitab 22.1. Analysis of Variance (ANOVA) was performed at a 95% confidence level to evaluate the statistical significance of linear, quadratic, and interaction terms. Only statistically significant terms were retained in the final predictive equations. Model adequacy was primarily evaluated using the adjusted coefficient of determination (adjusted R^2), which accounts for the number of predictors included in the regression model.

2.2 Specimen Fabrication

All specimens were fabricated using an Anycubic Photon Mono MSLA printer with ABS Photosensitive Resin. The specimen geometry was developed in Autodesk Tinkercad and exported as an STL file prior to slicing in Chitubox Basic V2, where process parameters were assigned according to the CCD matrix presented in Table 2. Build orientation and placement were kept constant to avoid introducing uncontrolled geometric variability.

Notably, two specimen geometries were produced for different experimental evaluations. For compression testing, rectangular prism specimens with dimensions 25.4 mm × 12.7 mm × 12.7 mm were fabricated in accordance with ASTM D695 requirements for rigid plastics. This geometry provides a 2:1 aspect ratio, ensuring stable compressive loading. For ultrasonic evaluation, cubic specimens measuring 30 mm × 30 mm × 30 mm were printed to enable wave propagation assessment along the x, y, and z directions.
The CCD generated 20 distinct parameter combinations. For compression testing, five replicate specimens were fabricated and tested for each parameter combination, resulting in a total of 100 compression specimens. For ultrasonic evaluation, one cube specimen was produced for each parameter combination, yielding 20 ultrasonic specimens.

Following fabrication, specimens were rinsed in isopropyl alcohol and post-cured under UV light at 400 nm and an irradiance of approximately 10–15 mW/cm^2 for 20 minutes. Note that the ambient temperature during printing was maintained at 23 ± 2°C.

2.3 Compression Testing

Mechanical properties were evaluated using a universal testing machine equipped with a 10 kN load cell. Consequently, compression testing was conducted in accordance with ASTM D695. Rectangular specimens were positioned concentrically between the compression platens to ensure uniform axial loading and minimize eccentricity.

Specifically, the crosshead speed was 1.3 mm/min. Load and displacement were recorded continuously throughout testing, and the data-acquisition rate was maintained in accordance with ASTM guidelines to ensure accurate capture of the elastic region and the peak stress response.

Compressive strength was calculated using Eq. (1):

$$\sigma_C = \frac{F_{max}}{A} \quad (1)$$

where F_{max} is the maximum recorded load, and A is the original crosssectional area of the specimen. For each of the 20 parameter combinations, five replicate tests were conducted. The average compressive strength for each parameter combination was used as the response input for regression modeling.

2.4 Ultrasonic Testing and Attenuation Measurement

The subsection headings should be numbered in Arabic numerals such as 2.1, 3.1, etc. The figures and tables should be numbered consecutively and inserted within the text. The captions for figure should be placed below the illustrations, whereas the captions for tables should be placed above the table content. Both captions should be typed in Palatino Linotype, font size 10. If the discussions need to be arranged in point form, Roman numeral format is preferred such as below.

Figure 1: Acoustic characterization setup

UT procedures followed the general guidance of ASTM E1065 for ultrasonic search unit evaluation and ASTM E494 for ultrasonic velocity measurement. Cubic specimens (30 mm × 30 mm × 30 mm) were used to evaluate wave propagation along the print build-up direction (x-axis). Correspondingly, the actual specimen thickness used for velocity calculations was measured using a digital calliper.

Longitudinal wave velocity was calculated using Eq. (2):

$$V = \frac{2d}{\Delta t} \quad (2)$$

where d represents specimen thickness, and Δt represents the measured round-trip travel time. Specific attenuation was determined from amplitude measurements using Eq. (3):

$$\alpha(\text{dB/mm}) = 20\log\left(\frac{a_0}{a_i}\right)/d \quad (3)$$

where a_0 represents the first backwall echo and a_i represents the second backwall echo. For each parameter combination, ultrasonic measurements were repeated three times to ensure consistency, and the averaged values were used for regression modeling.

3.0 RESULTS AND DISCUSSION

The measured values of compressive strength (MPa), ultrasonic attenuation (dB/mm), and sound velocity (m/s) obtained from the twenty experimental runs are summarized in Table 2. These responses represent the key performance characteristics of the fabricated wedge specimens. Compressive strength reflects the mechanical integrity of the material, ultrasonic attenuation describes the acoustic energy loss during wave propagation, and sound velocity governs the calibration behavior of the wedge in UT applications.

Thus, to examine the influence of SLA printing parameters on these responses, the experimental results were first analyzed using graphical response trends in main effects plots. These plots illustrate how the process parameters, LH, ET, and LD, affect the measured responses and provide an initial interpretation of the parameter influence. The interaction of the parameters on the mechanical and acoustic responses is discussed in Section 3.1.

Since an effective ultrasonic wedge material must simultaneously exhibit high mechanical strength and efficient acoustic transmission, the combined mechanical–acoustic performance of the printed specimens was further evaluated in Section 3.2. Finally, the influence of the process parameters on ultrasonic wave velocity is discussed in Section 3.3 with respect to its role in wedge calibration and ultrasonic inspection performance.

Table 2: Measured responses of compressive strength (MPa), ultrasonic attenuation (dB), and sound velocity (m/s) for all 20 experimental runs

Run	Layer Height, LH (mm)	Exposure Time, ET (s)	Light-off Delay, LD (s)	Compressive Strength (MPa)	Attenuation (dB/mm)	Velocity (m/s)

1	0.01	0.001	0	49.82	0.0949	2107
2	0.2	0.001	0	22.03	0.0403	2150
3	0.01	0.1	0	23.72	0.0141	1962
4	0.2	0.1	0	22.64	0.0384	2138
5	0.01	0.001	0.1	40.57	0.0824	2112
6	0.2	0.001	0.1	42.68	0.0647	1979
7	0.01	0.1	0.1	47.42	0.0841	2105
8	0.2	0.1	0.1	43.83	0.0649	2019
9	0.01	0.0505	0.05	38.41	0.0399	2121
10	0.2	0.0505	0.05	42.53	0.0647	2135
11	0.105	0.001	0.05	52.63	0.1462	1995
12	0.105	0.1	0.05	40.72	0.0920	1979
13	0.105	0.0505	0	47.02	0.1330	1975
14	0.105	0.0505	0.1	77.38	0.0937	1974
15	0.105	0.0505	0.05	68.54	0.0909	2123
16	0.105	0.0505	0.05	79.36	0.1100	2114
17	0.105	0.0505	0.05	79.41	0.1741	1996
18	0.105	0.0505	0.05	73.63	0.1121	1996
19	0.105	0.0505	0.05	79.44	0.1535	2100
20	0.105	0.0505	0.05	68.47	0.0580	2104

3.1 Influence of Printing Parameters on Mechanical and Acoustic Properties

The influence of LH, ET, and LD on compressive strength, ultrasonic attenuation, and wave velocity is illustrated in the main effects plots in Figures 2, 3, and 4, respectively. Specifically, these plots provide a direct visualization of how each SLA process parameter influences the mechanical and acoustic behavior of the printed specimens.

For compressive strength, as depicted in Figure 2, both LH and ET exhibit nonlinear trends, with peak values near intermediate parameter levels. Increasing LH from 0.01 mm to approximately 0.10 mm improved compressive strength by enhancing curing overlap and stronger interlayer bonding between successive layers. However, further increases in LH reduce the effectiveness of interlayer fusion, thereby lowering mechanical strength. This behavior has been widely reported in SLA studies where layer thickness significantly affects the mechanical performance of printed parts by varying interlayer bonding quality [33].

Moreover, the attenuation response in Figure 3 illustrates a trend different from that of the compressive strength. The main effects plot indicates that LH had the strongest influence, with attenuation peaking near the intermediate LH level and decreasing toward both lower and higher LH values. This behavior is associated with the microstructural characteristics generated during the layer-by-layer fabrication process. Increased interlayer interfaces and internal heterogeneities can enhance ultrasonic scattering and viscoelastic damping, thereby increasing attenuation [34, 35].

The velocity response in Figure 4 demonstrates moderate dependence on LH, with smaller variations observed for ET and LD. Ultrasonic wave velocity in polymeric materials is primarily governed by the elastic stiffness, density, and viscoelastic behavior of the material. Therefore, changes in curing conditions during SLA printing can slightly modify the internal microstructure and influence the propagation speed of ultrasonic waves [36].

Overall, the main effects plots indicate that LH is the dominant parameter affecting both mechanical and acoustic responses of the SLA-printed specimens. The intermediate LH region exhibited higher compressive strength and greater ultrasonic attenuation, suggesting a potential trade-off between mechanical integrity and acoustic transmission efficiency. These observations motivate the combined mechanical–acoustic evaluation using the MAI discussed in the following section.

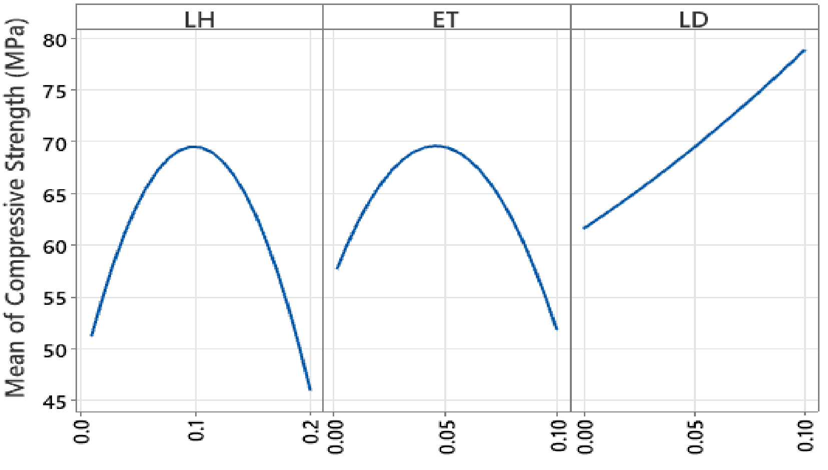

Figure 2: Main effects of Layer Height (LH), Exposure Time (ET), and Light-off Delay (LD) on the compressive strength of the SLA-printed specimens

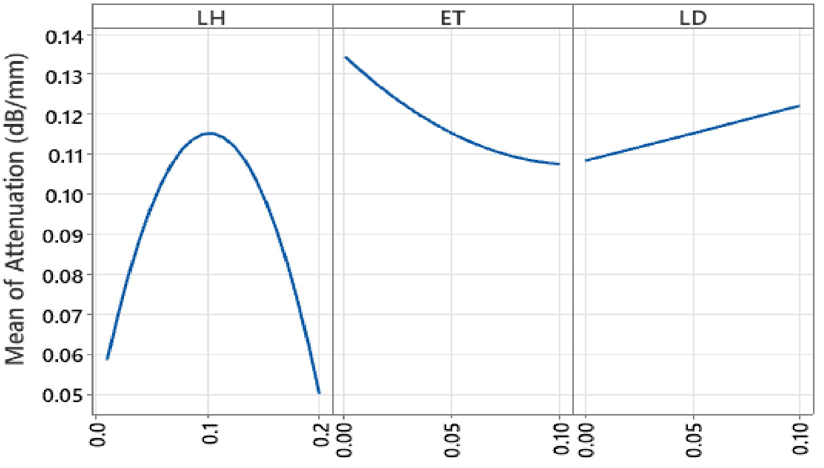

Figure 3: Main effects of Layer Height (LH), Exposure Time (ET), and Light-off Delay (LD) on ultrasonic attenuation of the SLA-printed specimens

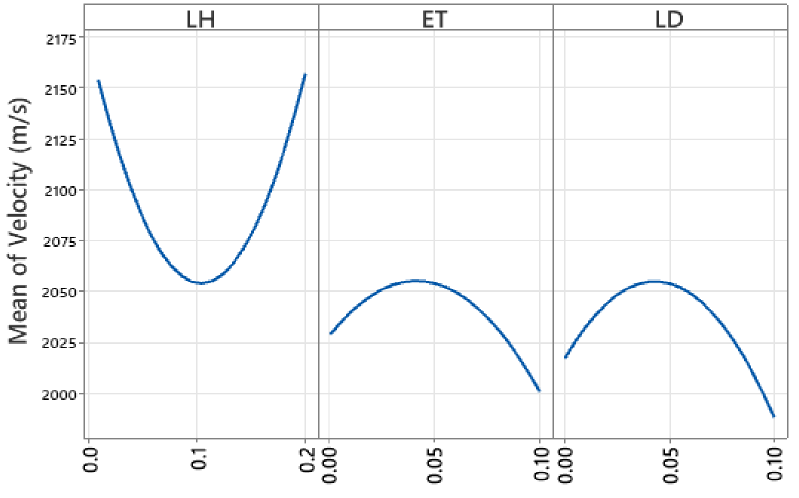

Figure 4: Main effects of Layer Height (LH), Exposure Time (ET), and Light-off Delay (LD) on ultrasonic wave velocity of the SLA-printed specimens
Figure 5: Relationship between compressive strength and ultrasonic attenuation for all experimental runs, grouped by Layer Height (LH)

3.2 Mechanical–Acoustic Performance Trade-off

For ultrasonic wedge applications, the material must provide sufficient mechanical integrity while maintaining low acoustic attenuation to ensure efficient ultrasonic transmission. The relationship between compressive strength and ultrasonic attenuation for all experimental runs is illustrated in Figure 5. A general positive trend is observed, as specimens with higher compressive strength tend to exhibit greater attenuation.

This behavior is associated with the curing characteristics of photopolymer materials during SLA. The observed increase in mechanical strength with increased curing is consistent with the

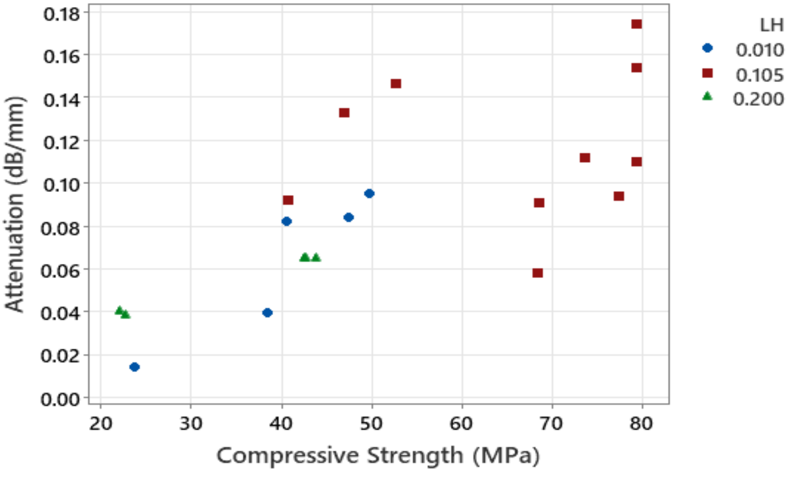

findings reported in [31], which attributed the improvement to enhanced interlayer bonding and increased cross-link density in the polymer network. However, the corresponding increase in ultrasonic attenuation is also consistent with the mechanism described in [34], where increased stiffness and internal microstructural heterogeneity can promote ultrasonic energy dissipation through scattering and viscoelastic damping during wave propagation. These findings therefore suggest that the observed mechanical strengthening with increased curing is accompanied by a moderate increase in ultrasonic attenuation.

The mean values summarized in Table 3 further highlight this mechanical–acoustic trade-off. The intermediate LH (0.105 mm) produced the highest average compressive strength (66.66 MPa) and resulted in the highest attenuation (0.116 dB/mm). Conversely, the largest LH (0.20 mm) yielded the lowest attenuation (0.055 dB/mm) but significantly lower mechanical strength (34.74 MPa). Notably, similar trends were observed for ET and LD, where increased curing conditions generally improved mechanical strength while slightly increasing acoustic attenuation.

Table 3: Mean compressive strength and ultrasonic attenuation at each parameter level of Layer Height (LH), Exposure Time (ET), and Light-off Delay (LD)

Parameter	Level	Mean Strength (MPa)	Mean Attenuation (dB/mm)
Layer height (mm)	0.01	39.99	0.063
	0.105	66.66	0.116
	0.2	34.74	0.055
Exposure Time (s)	0.001	41.55	0.086
	0.0505	65.42	0.103
	0.1	35.67	0.059
Light-off Delay (s)	0	33.05	0.064
	0.05	62.31	0.104
	0.1	50.38	0.078

From a practical standpoint, ultrasonic wedge materials must maintain sufficient mechanical integrity to withstand probe loading and scanning pressure while minimizing signal loss along the transmission path. In polymer-based inspection components, attenuation coefficients below approximately 0.10 dB/mm are generally desirable to maintain adequate signal amplitude during ultrasonic inspection [34, 37]. Based on these considerations, moderate curing conditions, particularly LH between 0.01 and 0.10 mm, combined with intermediate ET, provide a balanced compromise between mechanical durability and acoustic transmission performance.

Overall, the results demonstrate that process conditions that maximize mechanical strength do not necessarily produce the most favorable acoustic transmission characteristics. Therefore, optimization of SLA parameters for ultrasonic wedge fabrication should consider both mechanical and acoustic performance simultaneously.

3.3 Ultrasonic Testing and Attenuation Measurement

Ultrasonic wave velocity is a crucial parameter in wedge-based ultrasonic inspection because it directly determines the refracted beam angle and therefore influences probe calibration accuracy [36]. Additionally, the measured ultrasonic velocities of the SLA-printed specimens ranged from approximately 1970 m/s to 2150 m/s, corresponding to a variation of about ±4% around the mean (2050 m/s). This relatively narrow velocity range indicates stable acoustic propagation behavior of the printed polymer material.

Subsequently, the influence of the printing parameters on ultrasonic velocity was evaluated using response surface regression analysis, and the resulting ANOVA is summarized in Table 4. The regression model was statistically significant (p=0.006) with a non-significant lack-of-fit (p=0.742), indicating that the model adequately describes the experimental data.

The resulting regression model expressed in coded variables is given by Eq. (4):

$$V = 2048.8 + 86.8\,LH^2 - 66.0\,LD^2 - 54.7(LH \times LD) \qquad (4)$$

where V is the ultrasonic velocity (m/s), and LH and LD represent the coded Layer Height and Light-off Delay.

Table 4: Analysis of Variance (ANOVA) for the stepwise regression model describing ultrasonic velocity

Source	DF	Adj SS	Adj MS	F-Value	P-Value
Model	3	48990	16330	6.06	0.006
Square	2	25082	12541	4.65	0.026
LH*LH	1	24106	24106	8.95	0.009
LD*LD	1	13958	13958	5.18	0.037
2-Way Interaction	1	23908	23908	8.87	0.009
LH*LD	1	23908	23908	8.87	0.009
Error	16	43111	2694		
Lack-of-Fit	11	25411	2310	0.65	0.742
Pure Error	5	17700	3540		
Total	19	92102			

The response surface depicted in Figure 6 illustrates the combined influence of LH and LD on ultrasonic velocity, with ET fixed at the center level. The surface demonstrates a mild saddle-shaped pattern, suggesting a nonlinear interaction between the parameters. However, the overall velocity variation remains relatively small (ΔV = 180 m/s) across the investigated parameter space.

Figure 6: Combined influence of Layer Height (LH) and Light-off Delay (LD) on ultrasonic velocity, with Exposure Time (ET) fixed at the center level

Ultrasonic wave velocity in solids is primarily governed by the elastic modulus and density of the material [38]. Therefore, the observed velocity variation is likely associated with minor changes in curing-induced stiffness and interlayer bonding within the printed polymer structure. Since the velocity difference across all experimental conditions is limited to approximately 180 m/s, the nonlinear response observed in the regression model does not significantly affect the practical calibration of the ultrasonic wedge.

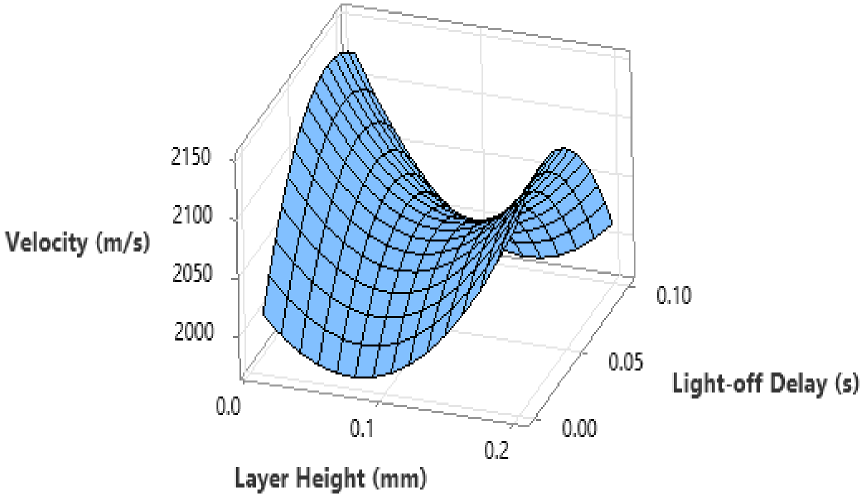

Consequently, the regression model obtained in this study can be used as a practical estimator of wedge velocity based on the selected printing parameters, allowing an approximate velocity value to be determined prior to final calibration using standard ultrasonic reference procedures [34].

The combined results from Sections 3.1–3.3 demonstrate that SLA process parameters influence both the mechanical integrity and acoustic transmission characteristics of the printed wedge material. Although intermediate curing conditions provide a favorable balance between compressive strength and ultrasonic attenuation, the ultrasonic velocity remains relatively stable across the investigated parameter space. Thus, this behavior indicates that SLA printing parameters can be optimized primarily based on mechanical–acoustic performance. Simultaneously, velocity calibration can be reliably estimated within a narrow range using the proposed regression model. These findings provide a practical guideline for the design and fabrication of SLA-printed ultrasonic wedges for NDT applications.

4.0 CONCLUSION

The objectives of this study were achieved through the systematic evaluation of the effects of SLA process parameters on compressive strength, ultrasonic velocity, and attenuation, as well as the relationship between mechanical and acoustic performance. The results demonstrate that the investigated printing parameters significantly influence mechanical strength and ultrasonic attenuation, while ultrasonic velocity remains relatively stable within the investigated parameter range. The main findings are summarized as follows:

- Compressive strength was strongly influenced by the printing parameters, ranging from 22 MPa to 79 MPa, with intermediate curing conditions providing the highest mechanical performance due to improved interlayer bonding.
- Ultrasonic attenuation ranged from approximately 0.04 dB/mm to 0.17 dB/mm and generally increased with mechanical strength, indicating a trade-off between mechanical integrity and acoustic transmission.
- Ultrasonic velocity remained relatively stable across the investigated parameter space, ranging from 1970 m/s to 2150 m/s (≈ ±4% variation), indicating that SLA parameters have a limited influence on wave propagation speed.
- A regression model based on LH and LD was developed to estimate ultrasonic velocity, serving as an initial estimator of wedge velocity prior to final experimental calibration.
- Overall, the results demonstrate that SLA process parameters can be optimized primarily based on mechanical–acoustic performance. Ultrasonic velocity can be reliably calibrated within a narrow range, supporting the feasibility of SLA-printed wedges for ultrasonic NDT applications.

ACKNOWLEDGMENTS

This research was not funded by any grant. Portions of the manuscript's language were edited using ChatGPT (version 5.2).

AUTHOR CONTRIBUTIONS

M.N.F. Saniman: Conceptualization, Methodology, Supervision, Formal Analysis, Writing – Original Draft Preparation; S.A. Zulkifli: Investigation, Data Curation, Formal Analysis, Software; M.R. Rahim: Supervision, Methodology, Writing – Review and Editing; A. Zhahir: Validation, Formal Analysis, Writing – Review and Editing; A. Ibrahim: Conceptualization, Validation, Writing – Review and Editing; M.H. Muhammad Sidik: Validation, Supervision, Writing – Review and Editing.

CONFLICTS OF INTEREST

The manuscript has not been published elsewhere and is not under consideration by other journals. All authors have approved the review, agree with its submission and declare no conflict of interest on the manuscript.

REFERENCES

[1] F. Honarvar and A. Varvani-Farahani, "A review of ultrasonic testing applications in additive manufacturing: Defect evaluation, material characterization, and process control," *Ultrasonics*, vol. 108, pp. 106227, 2020.

[2] P. Wang, L. Zhou, G. Liu, and Y. Pei, "In situ near-field microwave characterization and quantitative evaluation of phase change inclusion in honeycomb composites," *NDT & E International*, vol. 121, pp. 102469, 2021.

[3] A.O. Keim, P.P. Pandit, L.D. Sotelo, and M.S. McClain, "Nondestructive evaluation of material properties in polymer additive manufacturing processes: moving towards process-agnostic qualification," *Virtual and Physical Prototyping*, vol. 20, no. 1, 2025.

[4] A. Amin, D.A. Jack, P.K. Ravindranath, and T.J. Fleck, "Nondestructive quantification of internal raster path for additively manufactured components via ultrasonic testing," *Scientific Reports*, vol. 14, no. 1, pp. 11416, 2024.

[5] I. Malashin, V. Tynchenko, D. Martysyuk, N. Shchipakov, N. Krysko, M. Degtyarev, V. Nelyub, A. Gantimurov, A. Borodulin, and A. Galinovsky, "Assessment of Anisotropic Acoustic Properties in Additively Manufactured Materials: Experimental, Computational, and Deep Learning Approaches," *Sensors*, vol. 24, no. 14, pp. 4488, 2024.

[6] A.J. Balvantin, E. Rojas-Mancera, V.A. Ramirez, J.A. Diosdado-De-La-Pena, P.A. Limon-Leyva, and R.A. Figueroa-Diaz, "The Suitability of Using 3D PLA Printed Wedges for Ultrasonic Wave Propagation," *IEEE Access*, vol. 8, pp. 15205–15209, 2020.

[7] M. Pagac, J. Hajnys, Q.-P. Ma, L. Jancar, J. Jansa, P. Stefek, and J. Mesicek, "A Review of Vat Photopolymerization Technology: Materials, Applications, Challenges, and Future Trends of 3D Printing," *Polymers*, vol. 13, no. 4, pp. 598, 2021.

[8] S. Subedi, S. Liu, W. Wang, S.M.A. Naser Shovon, X. Chen, and H.O.T. Ware, "Multi-material vat photopolymerization 3D printing: a review of mechanisms and applications," *npj Advanced Manufacturing*, vol. 1, no. 1, pp. 9, 2024.

[9] H. Quan, T. Zhang, H. Xu, S. Luo, J. Nie, and X. Zhu, "Photo-curing 3D printing technique and its challenges," *Bioactive Materials*, vol. 5, no. 1, pp. 110–115, 2020.

[10] Y. Li, Q. Mao, J. Yin, Y. Wang, J. Fu, and Y. Huang, "Theoretical prediction and experimental validation of the digital light processing (DLP) working curve for photocurable materials," *Additive Manufacturing*, vol. 37, pp. 101716, 2021.

[11] M. Štaffová, F. Ondreáš, J. Svatík, M. Zbončák, J. Jančář, and P. Lepcio, "3D printing and post-curing optimization of photopolymerized structures: Basic concepts and effective tools for improved thermomechanical properties," *Polymer Testing*, vol. 108, pp. 107499, 2022.

[12] A. Milovanović, M. Montanari, Z. Golubović, M.P. Mărghitaş, A. Spagnoli, R. Brighenti, and A. Sedmak, "Compressive and flexural mechanical responses of components obtained through mSLA vat photopolymerization technology," *Theoretical and Applied Fracture Mechanics*, vol. 131, pp. 104406, 2024.

[13] A.M.G. Cheadle, E. Maier, W.M. Palin, P.L. Tomson, G. Poologasundarampillai, and M.A. Hadis, "The impact of modifying 3D printing parameters on mechanical strength and physical properties in vat photopolymerisation," *Scientific Reports*, vol. 15, no. 1, pp. 12592, 2025.

[14] M.N.F. Saniman, M.H. M Hashim, K.A. Mohammad, K.A. Abd Wahid,

W.M. Wan Muhamad, and N.H. Noor Mohamed, "Tensile Characteristics of Low Density Infill Patterns for Mass Reduction of 3D Printed Polylactic Parts," *International Journal of Automotive and Mechanical Engineering*, vol. 17, no. 2, pp. 7927–7934, 2020.

[15] N.P. Lee, R.A. Hamid, S. Maidin, N. Hajar, and T. Ito, "Effect of process parameters on tensile strength of 3D printed PLA parts," *Journal of Advanced Manufacturing Technology (JAMT)*, vol. 18, no. 3, 2024.

[16] J. Saini, L. Dowling, J. Kennedy, and D. Trimble, "Investigations of the mechanical properties on different print orientations in SLA 3D printed resin," *Proceedings of the Institution of Mechanical Engineers, Part C: Journal of Mechanical Engineering Science*, vol. 234, no. 11, pp. 2279–2293, 2020.

[17] C. Riccio, M. Civera, O. Grimaldo Ruiz, P. Pedullà, M. Rodriguez Reinoso, G. Tommasi, M. Vollaro, V. Burgio, and C. Surace, "Effects of Curing on Photosensitive Resins in SLA Additive Manufacturing," *Applied Mechanics*, vol. 2, no. 4, pp. 942–955, 2021.

[18] F. Pehlivan, "Enhancing tensile properties of polymer-based triply periodic minimal surface metamaterial structures: Investigating the impact of post-curing time and layer thickness via response surface methodology," *Polymer Engineering & Science*, vol. 64, no. 12, pp. 5915–5928, 2024.

[19] J.C. Young, S.A. Brinckmann, R.S. Fertig III, S.P. Lynch, and C.P. Frick, "Influence of layer thickness and exposure on mechanical properties of additively manufactured polymer-derived SiOC ceramics," *Open Ceramics*, vol. 19, pp. 100652, 2024.

[20] D.A. Yosef, T.A. ENAB, and I. Eldesouky, "Tribological and hardness characteristics of resin materials in masked stereolithography: impact of washing solution and curing time," *Progress in Additive Manufacturing*, vol. 11, no. 1, pp. 83–94, 2026.

[21] N. Vidakis, M. Petousis, V.M. Papadakis, and N. Mountakis, "Multifunctional Medical Grade Resin with Enhanced Mechanical and Antibacterial Properties: The Effect of Copper Nano-Inclusions in Vat Polymerization (VPP) Additive Manufacturing," *Journal of Functional Biomaterials*, vol. 13, no. 4, pp. 258, 2022.

[22] E.A. Garcia, C. Ayranci, and A.J. Qureshi, "Material Property-Manufacturing Process Optimization for Form 2 Vat-Photo Polymerization 3D Printers," *Journal of Manufacturing and Materials Processing*, vol. 4, no. 1, pp. 12, 2020.

[23] P. Turek, A. Bazan, P. Kubik, and M. Chlost, "Development of a Calibration Procedure of the Additive Masked Stereolithography Method for Improving the Accuracy of Model Manufacturing," *Applied Sciences*, vol. 15, no. 13, pp. 7412, 2025.

[24] T.F. de Oliveira, A.C.M. Cavalheiro, F. Buiochi, M.S.G. Tsuzuki, J.P. Leão-Neto, G.C. Silva, G.T. Silva, and J. Henrique Lopes, "Ultrasonic characterization of 3D-printed polymer objects," *Ultrasonics*, vol. 149, pp. 107572, 2025.

[25] M. Gattin, N. Bochud, G. Rosi, Q. Grossman, D. Ruffoni, and S. Naili, "Ultrasound characterization of the viscoelastic properties of additively manufactured photopolymer materials," *The Journal of the Acoustical Society of America*, vol. 152, no. 3, pp. 1901–1912, 2022.

[26] C.K.P. Vallabh, Y. Zhang, and X. Zhao, "In-situ ultrasonic monitoring for Vat Photopolymerization," *Additive Manufacturing*, vol. 55, pp. 102801, 2022.

[27] S. Jamshididana, D.J. Roach, and D. Roach, "In-Situ Ultrasonic Monitoring for Process Monitoring of Digital Light Process 3D Printing.", in *Proceedings of the 15th International Workshop on Structural Health Monitoring, Destech Publications, Inc.*, 2025.

[28] M.N.F. Saniman, M.I. Yahya, N.N. Mahmud, K.A. Abd Wahid, K.A. Mohammad, N.F. Che Harun, M.H. Sakir, and M. Khairudin, "3D Printing Parameters Optimization of ABS Probe Holder for Ultrasonic Scanner," *Journal of Advanced Research in Applied Sciences and Engineering Technology*, vol. 48, no. 2, pp. 10–15, 2024.

[29] M. Bakaric, P. Miloro, A. Javaherian, B.T. Cox, B.E. Treeby, and M.D. Brown, "Measurement of the ultrasound attenuation and dispersion in 3D-printed photopolymer materials from 1 to 3.5 MHz," *The Journal of the Acoustical Society of America*, vol. 150, no. 4, pp. 2798–2805, 2021.

[30] S.M.Z.S. Bukhari, M.A. Bukhari, and M. Hossain, "Vat Photopolymerization of Smart Polymers for Biomedical Applications," *ACS Applied Polymer Materials*, vol. 7, no. 18, pp. 12117–12144, 2025.

[31] B. Msallem, J.J. Vavrina, M. Beyer, F.S. Halbeisen, G. Lauer, A. Dragu, and F.M. Thieringer, "Dimensional Accuracy in 3D Printed Medical Models: A Follow-Up Study on SLA and SLS Technology," *Journal of Clinical Medicine*, vol. 13, no. 19, pp. 5848, 2024.

[32] M. Mehrpouya, A. Ghalayaniesfahani, J.F. Postmes, and I. Gibson, "Tailoring mechanical properties in 3D printed multimaterial architected structures," *Journal of the Mechanical Behavior of Biomedical Materials*, vol. 152, pp. 106431, 2024.

[33] K. Chockalingam, N. Jawahar, and U. Chandrasekhar, "Influence of layer thickness on mechanical properties in stereolithography," *Rapid Prototyping Journal*, vol. 12, no. 2, pp. 106–113, 2006.

[34] K. Ono, "A Comprehensive Report on Ultrasonic Attenuation of Engineering Materials, Including Metals, Ceramics, Polymers, Fiber-Reinforced Composites, Wood, and Rocks," *Applied Sciences*, vol. 10,

no. 7, pp. 2230, 2020.

[35] M.N.F. Saniman and I. Ihara, "Feasibility study on characterization of non-Gaussian rough surface by ultrasonic reflection method with the Kirchhoff theory," *Mechanical Engineering Journal*, vol. 3, no. 6, pp. 16-00162-16–00162, 2016.

[36] F. Lionetto, F. Montagna, and A. Maffezzoli, "Ultrasonic Dynamic Mechanical Analysis of Polymers," *Applied Rheology*, vol. 15, pp. 326–335, 2005.

[37] A. Bagheri and J. Jin, "Photopolymerization in 3D Printing," *ACS Applied Polymer Materials*, vol. 1, no. 4, pp. 593–611, 2019.

[38] I. Oral and M. Ekrem, "Measurement of the elastic properties of epoxy resin/polyvinyl alcohol nanocomposites by ultrasonic wave velocities," *Express Polymer Letters*, vol. 16, no. 6, pp. 591–606, 2022.